# ENERGY CONSERVATION IN LAGRANGE-REMAP MODELING FOR IDEAL-MHD SHOCK PROPAGATION (U)

John H. J. Niederhaus, Thomas A. Gardiner,
William J. Rider, and Allen C. Robinson

This paper was prepared for submittal to
Nuclear Explosives Code Developers Conference (NECDC) 2008
Livermore, CA
October 20 – 24, 2008

January, 2009

DISCLAIMER

**SAND-2008-8194C**
Approved for public release
distribution is unlimited

Title: **Energy conservation in Lagrange-remap simulations for ideal-MHD shock propagation (U)**

Authors: John H. J. Niederhaus, Thomas A. Gardiner, William J. Rider, and Allen C. Robinson

Submitted to: Nuclear Explosives Code Developers Conference (NECDC) 2008
Livermore, CA
October 21 – 24, 2009

# Energy conservation in Lagrange-remap simulations for ideal-MHD shock propagation (U)

**J. H. J. Niederhaus, T. A. Gardiner, W. J. Rider, and A. C. Robinson**
**Sandia National Laboratories**

*Two classical verification problems from shock hydrodynamics are adapted for verification in the context of ideal magnetohydrodynamics (MHD) by introducing strong transverse magnetic fields, and simulated using the finite element Lagrange-remap MHD code ALEGRA for purposes of rigorous code verification. The concern in these verification tests is that inconsistencies related to energy advection are inherent in Lagrange-remap formulations for MHD, such that conservation of kinetic and magnetic energy may not be maintained. Hence, total energy conservation may also not be maintained. MHD shock propagation may therefore not be treated consistently in Lagrange-remap schemes, as errors in energy conservation are known to result in unphysical shock wave speeds and post-shock states. That kinetic energy is not conserved in Lagrange-remap schemes is well known, and the correction of DeBar has been shown to eliminate the resulting errors. Here, the consequences of the failure to conserve magnetic energy are revealed using order verification in the two magnetized shock-hydrodynamics problems. Further, a magnetic analog to the DeBar correction is proposed and its accuracy evaluated using this verification testbed. Results indicate that only when the total energy is conserved, by implementing both the kinetic and magnetic components of the DeBar correction, can simulations in Lagrange-remap formulation capture MHD shock propagation accurately. (U)*

**Keywords:** hydrodynamics, MHD, verification, shock

## Introduction

In many applications for multiphysics modeling and simulation in solid dynamics, hydrodynamics, and magnetohydrodynamics (MHD), it is highly desirable to maintain a Lagrangian formulation while allowing the medium to move across a fixed Eulerian mesh. This is necessary in order to ensure optimal coupling to existing constitutive laws and equations of state, while also allowing for the development of strong shear and large distortions in the simulated flow fields, which could not be supported in purely Lagrangian schemes. This has commonly been accomplished using an operator-split approach in which the motion occurs in two stages: a Lagrangian step and an Eulerian advection or "remap" operation. In this Lagrange-remap mode, time evolves only during the Lagrangian step, and material moves relative to the mesh only in the remap step.

Typically, such Lagrange-remap schemes conserve the total mass, momentum, and internal energy in the simulation during the remap step, but kinetic energy, which in this case is a derived variable, is often not explicitly conserved, as noted by Benson (1992) (Section 3.6). Benson notes that since total energy is then also not conserved, significant errors may arise, particularly in the treatment of shock propagation. Although this problem has been addressed for the case of pure solid dynamics and hydrodynamics using the correction of DeBar (1974), in MHD, the additional component of the total energy associated with magnetic fluxes may also not be conserved during remap, leading to further errors. These errors can be deadly in simulations of MHD environments where strong shocks or stagnation phenomena are important, including Z-pinch wire-array implosions, solar wind and magnetosphere dynamics, and stellar accretion.

In the present study, the multiphysics finite-element code ALEGRA (see Robinson and Garasi, 2004, and Robinson *et al.*, 2008) is used to determine the significance of these errors in two classical shock-dominated problems adapted for use in ideal MHD. These problems include magnetized versions of the Noh shock problem (Noh, 1987) and the Woodward-Colella interacting blast wave problem (Woodward and Colella, 1984). Further, following the approach of DeBar (1974), an algorithm is implemented in ALEGRA for maintaining conservation of total energy, including both kinetic and magnetic energy. Its effect on solution accuracy and convergence for these problems is investigated using standard methods of code verification.

**Lagrange-remap formulation for ideal MHD**

Ideal MHD describes the motion of a perfectly conducting, inviscid continuum in the presence of magnetic fields; displacement currents, electrical resistivity, thermal conduction, and momentum diffusion are all neglected. These approximations yield the following system of conservation laws for mass, momentum, energy, and magnetic flux:

$$\frac{\partial \rho}{\partial t} + \nabla \cdot (\rho \mathbf{V}) = 0 \tag{1}$$

$$\frac{\partial \mathbf{V}}{\partial t} + (\mathbf{V} \cdot \nabla)\mathbf{V} + \frac{1}{\rho}\nabla p - \frac{1}{\rho}(\nabla \times \mathbf{B}) \times \mathbf{B} = 0 \tag{2}$$

$$\frac{\partial \varepsilon}{\partial t} + (\mathbf{V} \cdot \nabla)\varepsilon + \frac{p}{\rho}(\nabla \cdot \mathbf{V}) = 0 \tag{3}$$

$$\frac{\partial \mathbf{B}}{\partial t} - \nabla \times (\mathbf{V} \times \mathbf{B}) = 0\,, \tag{4}$$

where $\rho$ is the density, $\mathbf{V}$ is the velocity, $p$ is the pressure, $\mathbf{B}$ is the magnetic flux density, and $\varepsilon$ is the internal energy density. This nonlinear hyperbolic system, whose Jacobian matrix has real eigenvalues, admits discontinuous solutions, with MHD waves propagating at speeds corresponding to the seven eigenvalues, as has been described in detail by Ryu and Jones (1995) and Roe and Balsara (1996).

The multiphysics finite-element code ALEGRA integrates the full system of equations for resistive MHD forward in time using an operator-split framework, in which the solution update occurs in two stages: a Lagrangian step and an Eulerian advection or "remap" operation. Time evolves only in the Lagrangian step, during which material and mesh motion occurs, and other physical processes in the simulation may be individually updated as well. Initially, the Lagrangian equations of motion, with thermodynamic and magnetic stresses and source terms computed from the previous cycle, are integrated in a moving frame, using a time-staggered finite-element discretization. These governing equations may be written as

$$\dot{\mathbf{x}} = \mathbf{V} \tag{5}$$

$$\frac{\partial \rho}{\partial t} + \nabla \cdot (\rho \mathbf{V}) = 0 \tag{6}$$

$$\rho \frac{\partial \mathbf{V}}{\partial t} = \nabla \cdot \left(\mathbf{T} + \mathbf{T}^{M}\right) + \mathbf{b} \tag{7}$$

$$\rho \frac{\partial \varepsilon}{\partial t} = \mathbf{T} \cdot \nabla \mathbf{V} + S_e \tag{8}$$

$$\frac{\partial \mathbf{B}}{\partial t} - \nabla \times \left( \mathbf{V} \times \mathbf{B} \right) = 0 , \tag{9}$$

where **x** is the coordinate, **T** and $\mathbf{T}^M$ are the thermodynamic and magnetic stresses, respectively, **b** represents body forces, and $S_e$ represents energy sources. Physical dissipative mechanisms are neglected in this "ideal-MHD" component of the Lagrangian step, though artificial viscosity is included as a contributor to the simulated stresses.

Subsequently, magnetic diffusion is incorporated by solving a transient boundary-value problem on the deformed Lagrangian mesh, as described by Robinson and Garasi (2004). Other processes including radiation transport and thermal conduction are similarly updated by solving linear elliptic systems on the deformed mesh. The stress tensors are then computed and evaluated at element centers as a contribution to the stresses from which the nodal forces are assembled in the finite element formulation (see Robinson *et al.*, 2008). However, the code may be run in an "ideal-MHD" mode, where these dissipative mechanisms are excluded by omitting each of these updates. In this mode, the coupling between the material motion and the magnetic field is unaffected by magnetic diffusion or Joule heating (which do not appear in Equations 2 and 4), and computed solutions should satisfy Equations 1-4. This mode represents the foundational component of the MHD treatment in ALEGRA, and is of interest from the perspective of code verification because underlying inconsistencies in implementation that are obscured by dissipative effects in modeling non-ideal systems are exposed in the ideal-MHD mode.

Of particular interest here are inconsistencies in energy conservation that arise as a result of the remap operation, subsequent to the Lagrangian step just described. In the remap operation, which is intended to be conservative, the degrees of freedom are mapped from the deformed Lagrangian mesh onto an arbitrary nearby mesh, which, in Eulerian mode, is the original mesh prior to the Lagrangian step. Though ALEGRA may be run in the purely Lagrangian formulation, many problems in the application space of ALEGRA and similar codes must be treated using an Eulerian reference frame, so that large deformations, shear, and vorticity may be captured accurately. The Lagrange-remap formulation allows the simulation to proceed in an Eulerian frame, while maintaining the capacity to update material states using constitutive relations formulated for motion in the Lagrangian frame.

The remap step in ALEGRA moves mass, momentum, and internal energy on quadrilateral and hexahedral elements from the Lagrangian to the Eulerian (or nearby arbitrary) mesh using a second-order conservative advection method, as described by Peery and Carroll (2000). The advection scheme incorporates, by default, the second-order-accurate, monotonicity-preserving method of Van Leer (1979) in computing fluxes, and uses Benson's half interval shift (HIS) algorithm (Benson, 1992b) to remap staggered mesh variables. As user options, a third-order method may be used, or a first-order donor method with or without a minmod limiter may be used. Multidimensional remap is performed in a sequence of one-dimensional passes, whose ordering is permuted on each cycle. The mass is remapped in the volume-based coordinate, and all other conserved variables are remapped using the mass-based coordinate, weighted by the remapped mass (Robinson *et al.*, 2008). In the case of multimaterial problems, any of a number of interface reconstruction algorithms (*e. g.* SMYRA, SLIC, and PIR – see Peery and Carroll, 2000; Dolbow *et al.*, 2008; and Mosso *et al.*, 2008) can be used to compute fluxes for each material.

As for the transient magnetic quantities, an extension of the constrained transport algorithm of Evans and Hawley (1988) is used to update the magnetic flux density while exactly

maintaining its divergence-free nature (div **B**=0). The magnetic flux is updated by taking advantage of the identity

$$\int_V (\nabla \cdot \mathbf{B}) dV = 0 = \int_{S=\partial V} \mathbf{B} \cdot \mathbf{da}\,, \tag{10}$$

where $V$ represents the volume element of which $S$ is the bounding surface, and **da** is the incremental outward normal area vector on $S$. The remap formulation is obtained by differencing Equation 10 over the course of the Lagrangian step and solving for the corresponding increment in the flux density by computing fluxes across each surface of the volume that is swept out by the deformation of the element during the Lagrangian step. This yields a remapped flux density that is divergence-free by construction, and provides natural upwinding. However, limiters are also applied to the face fluxes in order to maintain monotonicity.

It should be emphasized that only the nodal momenta, element-centered masses and internal energies, and face-centered magnetic fluxes are remapped and incorporated into the updated solution. (In the case of materials with strength, stresses must also be remapped.) These are the fundamental degrees of freedom that appear in the finite-element formulation. The post-remap kinetic energy, magnetic energy, and total energy are then derived quantities. As in a number of other Lagrange-remap codes (*e.g.* CTH – see McGlaun *et al.*, 1990), the code can be run in a mode that remaps kinetic energy as well, but only as a diagnostic monitor of energy conservation, and/or as a tool for modifying the energy in order to maintain total energy conservation, as described below.

**Kinetic and magnetic energy conservation in remap**

Such a diagnostic is needed in Lagrange-remap methods because it has been observed that the remap operation fails to conserve kinetic energy (see DeBar, 1974; McGlaun, 1990;Benson, 1992a; Pember and Anderson, 2000; and Youngs, 2007). Since the momentum is linear in the velocity, but the kinetic energy is quadratic in velocity, momentum and kinetic energy cannot be simultaneously advected in a way that is conservative. Further, because of the staggered discretization in the finite element method, which computes velocities at nodes and internal energies at element centers, a statement that requires conservation of total energy would not be self-consistent. Instead, element-centered internal energy alone is conserved in remap, and conservation of kinetic energy is no longer explicitly maintained. The kinetic energy may then vary relative to the value that would have resulted if it were remapped independently. Because kinetic energy is not conservatively advected in remap, the total energy in the simulation is not conserved. The consequences of failed energy conservation are many, but include in particular the development of unphysical shock wave speeds and jump conditions, especially in problems where large exchanges between kinetic, internal, and/or magnetic energy occur (*e.g.* stagnating flows and shock interactions).

Several approaches to mitigating this problem have been proposed and implemented in various codes, which are summarized by Benson (1992a) in Section 3.6. One of the most widely-used of these approaches is based on the scheme of DeBar (1974), who proposed explicitly computing the magnitude of kinetic energy discrepancy due to remap. Such a calculation can be written for the kinetic energy in an element as

$$\Delta E_k = \frac{1}{N}\sum_{n=1}^{N} \tfrac{1}{2}\mathrm{P}[m]\left(\mathrm{P}[\mathbf{V}_n]\cdot\mathrm{P}[\mathbf{V}_n]\right) - \mathrm{P}\left[\frac{1}{N}\sum_{n=1}^{N}\tfrac{1}{2}m(\mathbf{V}_n\cdot\mathbf{V}_n)\right], \tag{11}$$

where $m$ is the element mass, $n$ is an index of nodes associated with the element, and $N$ is the total number of nodes associated with the element. The notation P[.] heuristically represents the remap operator, such that P [**V**] denotes the velocity as measured after remap of momentum, and **V** the velocity before remap. In this so-called "DeBar fix" or "DeBar correction," the kinetic energy discrepancy $\Delta k$ in each element (which may take the form of deficit or surplus) is re-introduced to the calculation as internal energy in the element, so that the correspondence between conservation of momentum and conservation of energy in the element is restored. The DeBar correction has been applied successfully in a number of Lagrange-remap codes, including CTH (McGlaun *et al.*, 1990), TURMOIL3D (Youngs, 2007), and ALEGRA (Robinson *et al.*, 2008). However, it is important to note that multiple formulations of the expression given in Equation 11 are possible – particularly with regard to the weighting given to each node – and uniqueness of the solution is therefore lost.

For MHD flows, since the magnetic energy is quadratic in **B**, but the face-centered magnetic fluxes are linear in **B**, a similar discrepancy in the magnetic energy remains, even when the standard DeBar correction has been successfully implemented. Hence, total energy is still not conserved, and a magnetic extension to the DeBar correction is needed. Such an extension has been devised for ALEGRA. In this "magnetic DeBar correction" algorithm, the magnetic energy discrepancy arising during remap of the magnetic flux is computed explicitly in each element using the shape functions $\mathbf{F}_f$ and magnetic fluxes $\Phi_f$ on the faces. The magnetic flux $\Phi$ is the degree of freedom handled in the finite element method, defined as

$$\Phi_f = \int_S \mathbf{B}\cdot\mathbf{da}_f\,, \tag{12}$$

where $f$ is the face index, and $\mathbf{da}_f$ is the incremental outward normal area vector on face $f$. The magnetic energy is obtained by discretely integrating the magnetic flux over the face shape function, and then discretely integrating these face-integrated fluxes over the element's quadrature points using their weightings $w_q$. The magnetic energy in an element is discretely represented in ALEGRA as

$$E_m = \frac{1}{2\mu}\int_V \mathbf{B}\cdot\mathbf{B}dV \approx \frac{1}{2\mu}\sum_{q=1}^{Q}\left[w_q\left(\sum_{f=1}^{F}\Phi_f\mathbf{F}_f(\mathbf{x}_q)\right)^2\right], \tag{13}$$

where $\mu$ is the magnetic permeability, $dV$ is the incremental volume element, $F$ is the total number of faces associated with an quadrature point, and $\mathbf{x}_q$ is the coordinate of quadrature point $q$. The magnetic energy discrepancy arising during remap is then computed as

$$\Delta E_m = \frac{1}{2\mu}\sum_{q=1}^{Q}\left[w_q\left(\sum_{f=1}^{F}\mathrm{P}[\Phi_f]\mathbf{F}_f(\mathbf{x}_q)\right)^2\right] - \mathrm{P}[E_m], \tag{14}$$

where P[.] heuristically represents the remap operator. In the magnetic DeBar corretion, the magnetic energy density discrepancy $\Delta E_m$, like the kinetic energy density discrepancy, is restored to the element as internal energy after the remap step.

In this way, then, the magnetic energy is also advected conservatively in remap with the same accuracy as the magnetic flux density. With the full DeBar correction implemented, including both kinetic and magnetic components, all forms of energy are advected conservatively in remap, and the total energy should therefore be conserved in the calculation. It is anticipated that with total energy conserved by means of the full (kinetic + magnetic) DeBar correction, problems that include propagation and/or interaction of strong MHD shock waves will exhibit dramatically improved accuracy in shock wave speeds and jump conditions. Further, it is hypothesized that an accurate solution for these problems in the Lagrange-remap formulation may only be obtained by making use of the full DeBar correction algorithm. In order to test these hypotheses, and to determine whether thresholds or limits are needed in the DeBar correction, two verification problems from ideal MHD are proposed below.

**Verification methodology**

Two simple verification problem are proposed, based on classical shock-hydrodynamics problems found in the literature: the stagnation-flow shock problem of Noh (1978), and the interacting blast-wave problem of Woodward and Colella (1984). In both cases, very strong discontinuities in thermodynamic variables propagate in a one-dimensional domain, and the medium of propagation is an ideal gas. To convert these to MHD-shock problems, a uniform, oblique B-field is imposed, and the medium is assumed to have infinite conductivity, so that magnetic diffusion will not obscure the exchange of energy between various forms in the system. (In this case, the ideal-MHD mode is used in ALEGRA.) The magnitude of the imposed B field is chosen such that magnetic energy densities have the same order of magnitude as kinetic and internal energy densities. A series of similar ideal shock-MHD verification problems with exact solutions can be found in Ryu and Jones (1995), though the strength of the shocks arising in that set of problems is generally insufficient for the purposes of the present study.

Solutions at fixed time are computed for each problem using ALEGRA in various configurations, and analyzed using standard methods of code verification. For each case, a reference solution is generated, and *a posteriori* error estimates are made by computing error norms with respect to this solution. In the case of the magnetized Noh problem, an exact solution is computed using an ideal-MHD Riemann solver based on the method of characteristics (see Ryu and Jones, 1995). For the magnetized Woodward-Colella problem, the reference solution is an approximate solution obtained using the ideal-MHD Eulerian Godunov code *Athena* (see Gardiner and Stone, 2005 and Stone and Gardiner, 2007). However, as discussed below, care is taken to ensure that reference *Athena* solutions are generated on grids sufficiently fine to keep numerical errors at least an order of magnitude smaller than the smallest errors in the ALEGRA solutions.

*A posteriori* error estimates for the ALEGRA solutions make use of the $L_1$ norm for the density profile $\rho(x)$ at fixed time $t^*$. An $L_1$ norm, as opposed to an $L_2$ or $L\infty$ norm, is appropriate here because of the shock-dominated nature of these problems (see Lax, 1973 and Tadmore, 1998). The $L_1$ is the least dependent on solution smoothness, and therefore the most likely to provide a meaningful measure of error here. The continuous $L_q$ norm for density on the interval $a \le x \le b$ would be computed as

$$L_q[\rho(x)] = \left[ \frac{\int_a^b |\rho - \rho_R|^q \, dx}{\int_a^b \rho_R \, dx} \right]^{1/q}, \tag{15}$$

where $\rho_R$ denotes the reference solution. Here, we approximate the density error $e$ using the discrete $L_1$ norm, denoted by $\ell_1$, which we compute as

$$e = \ell_1[\rho] = \frac{\sum_{n=1}^{N} |\rho_n - \rho^*_{R,n}| \Delta x_n}{\overline{\rho}_R \sum_{n=1}^{N} \Delta x_n}, \tag{16}$$

where $\overline{\rho}_R$ is the volume-weighted mean density in the reference solution, $N$ is the number of data in the computed solution, $\Delta x_n$ is the $n$th interval length in the computed solution, and the reference value $\rho^*_{R,n}$ is obtained by evaluating $\rho_R$ at the element-center coordinate $x_n$. (Note that for node- or edge-centered variables such as the velocity, the nodal coordinate would be used.) For the present study, the reference solutions are regarded as piecewise constant, so that interpolation of the reference solution does not influence the error estimates. As an aside, it is important to note here that the volume weighting implied in Equation 16 is unnecessary in the case of Lagrange-remap simulations, which are effectively Eulerian, with uniform and constant volumes. However, volume weighting is imperative for computing error norms in pure Lagrangian simulations, particularly where strong shocks are involved.

The effective convergence rate $p$ is then computed for each fine/coarse simulation pair as

$$p = \frac{\ln\left( \frac{e^{\text{coarse}}}{e^{\text{fine}}} \right)}{\ln(2)}, \tag{17}$$

where it is assumed that $N_{\text{fine}}/N_{\text{coarse}}=2$. (For further discussion of solution comparison using such error norms and order-of-accuracy analysis, see Ober and Shadid, 2004.) For these two test problems, we expect ALEGRA solutions to exhibit no better than first-order convergence with $N$, due to the presence of singularities in the solution at shocks and contact discontinuities. As the mesh is refined, the $L_1$ norm, which is dominated by errors at singularities and proportional to the width of the regions where singularities are located, should diminish by a factor equal to the refinement ratio. Regardless of the accuracy of the method, this factor can be no greater than the first power of the refinement ratio. Further, Banks *et al.* (2008) have shown that for linearly degenerate waves, such as contact discontinuities, a convergence rate of no better than $r/(r + 1)$ can be expected for an $r$th-order discretization. Therefore, to the extent that errors at contact discontinuities contribute to the total error, we expect convergence rates significantly less than unity. Hence, our verification criteria must be based on the magnitude and distribution of the error, as well as the convergence rate, and convergence rates even as low as 1/2 may be interpreted as adequate. Negative or very small positive convergence rates, however, remain unacceptable.

**The magnetized Noh problem**

In the first of verification problems, the magnetized Noh problem, two sets of very strong constant velocity, constant-state MHD shocks are generated by bringing a very cold conducting medium to rest at a stagnation surface in the presence of an oblique magnetic field. The medium is an ideal gas with $\gamma$=5/3 and $c_V$=1. Two shocks propagate into the medium away from the stagnation surface in each direction, corresponding to the forward and backward fast- and slow-mode nonlinear MHD waves emanating from the initial discontinuity.

The problem is initialized on [0, 1] with a uniform initial thermodynamic state, but two regions of opposed motion, so that the stagnation surface forms at the interface between them at $x$=0.5:

$$\rho = 1.0$$
$$p = 1.0 \times 10^{-6}$$
$$T = p/\rho/(\gamma - 1) = 1.5 \times 10^{-6}$$
$$v_x = \begin{cases} 1.0 & x < 0.5 \\ -1.0 & x \geq 0.5 \end{cases}$$
$$v_y = v_z = 0$$
$$\mathbf{B} = \tfrac{1}{2}(\hat{x} + \hat{y}),$$

where $\hat{x}$ and $\hat{y}$ are the unit vectors in the $x$- and $y$-directions, and $T$ is the temperature. The problem is run to $t$=0.75. (In the Lagrangian case, the problem is initialized on [-0.75,1.75], such that at $t$=0.75, the medium has been compressed to approximately [0,1].) This is similar to the problem simulated by Noh (1978), except that the shock strength is not infinite (the gas has nonzero temperature and pressure at time zero), and a uniform, oblique field B=0.5 ($\hat{x} + \hat{y}$) is imposed. As the system evolves forward in time, shocks propagate outward from $x$=0.5 into the medium and convert a large portion of the kinetic and magnetic energy in the initial state into internal energy and transverse motion in the post-shock state. This transfer of energy between kinetic, magnetic, and internal energy, all of which have similar magnitudes in the post-shock state, is expected to provide a rigorous test of energy conservation in the ideal-MHD algorithm implemented in ALEGRA. It is important to note that, in a staggered discretization, where the velocities lie at the nodes, a simulation with an even number of uniform elements cannot initialize the $x$=0.5 velocity discontinuity in a problem such as this at an element edge, but at an element center, as will be noted below.

**Magnetized Noh problem setup.** For ease of computing exact solutions using a Riemann solver, the magnetized Noh problem is simulated with shocks emanating in both directions from an initial discontinuity in $x$-velocity $x$=0.5 (rather than simulating the half-space). The propagation of constant-velocity MHD shocks from the initial discontinuity in the magnetized Noh problem is shown in Figure 1, where ALEGRA results for this problem at $N$=512 are plotted in ($x$, $t$) space. The fast and slow MHD shocks can be identified in Figure 1 as the surfaces of discontinuity across which the fluid experiences an increase and decrease in $B_y$, respectively.

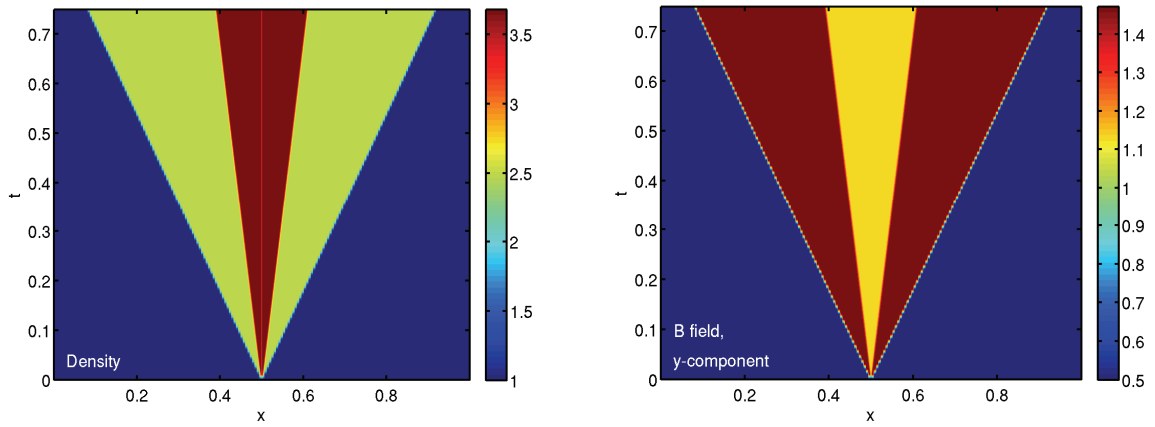


**Figure 1: ALEGRA results at N=512 for the magnetized Noh problem, plotted in (*x*,*t*) space. MHD shocks propagate outward from the stagnation surface near *x*=0.5. Left: density; right: *y*-component of B field.**

The problem is set up in ALEGRA on a uniform three-dimensional $N\times2\times2$ mesh, with hexahedral elements of aspect ratio 1. The shocks propagate in the $\pm x$-direction, and periodic boundary conditions are imposed in the *y*- and *z*- directions. Uniform and constant **B** and **V** fields are imposed at the ends of the domain (constant-*x* boundary surfaces), corresponding to the initial condition. We note that the specification of the correct boundary conditions for the transverse velocity on the ends of the domain is crucial to the success of the simulation: $v_y=v_z=0$ for $x=0,1$. Tensor artificial viscosity, with both linear and quadratic components, is included for shock capturing, with a linear coefficient of 0.5 and a quadratic coefficient of 2.0. It should be noted, however, that this artificial viscosity formulation is not fully consistent for ideal MHD, as dissipation is introduced only proportionally to gradients in the velocity magnitude, not gradients in transverse components of the velocity or the B field. For this problem, the Van Leer advection algorithm is used in the ALEGRA simulations.

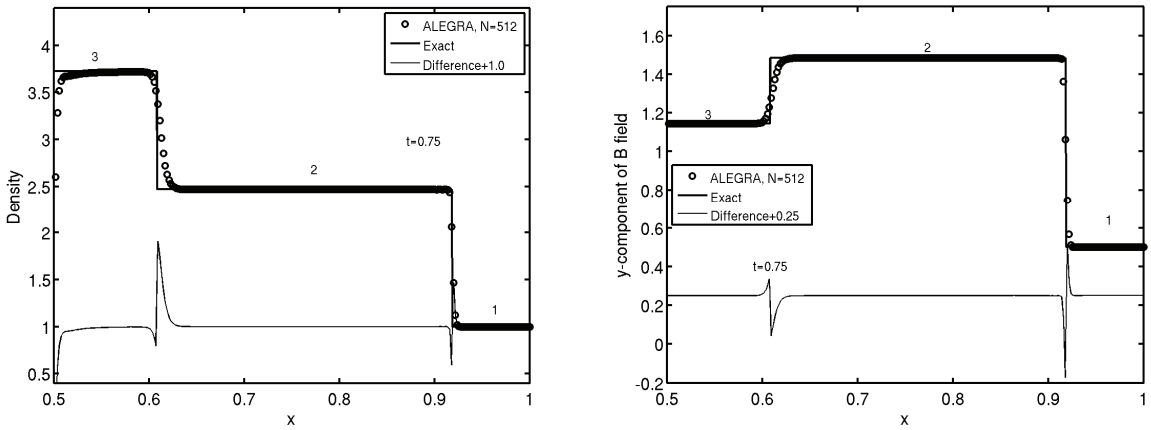


**Figure 2: Sample ALEGRA results at N=512 and t=0.75 for the forward half of the domain in the magnetized Noh problem, plotted with the exact solution, showing zones 1 (rightmost), 2, and 3 (leftmost). Left: density; right: *y*-component of B field. The difference between the two solutions is plotted as a lighter trace.**

The exact solution for this problem is computed using an ideal-MHD Riemann solver based on the method of characteristics (see Ryu and Jones, 1995). The exact solution at $t=0.75$ consists of five uniform states separated by discontinuities. The forward half of the domain is shown in Figure 2, including three of the five zones. Zone 1 is the unperturbed gas, with exact-solution

density $\rho_1$=1.0. Zone 2 contains gas that has interacted with the fast forward MHD shock: $\rho_2$=2.469. Zone 3 is the central zone and contains stagnant gas that has interacted with both the fast and slow MHD shocks: $\rho_3$=3.724.

**Energy conservation in the magnetized Noh problem.** As our primary interest here is to characterize inconsistencies that arise in energy conservation due to remap, and to evaluate the effectiveness of the measures taken to eliminate these inconsistencies, a convergence study sequence is performed in various remap configurations. (This is code verification; a known exact solution is available, and we measure error with respect to it, and the rate of convergence of the error.)

In each convergence study, the magnetized Noh simulation is run to $t$=0.75 for grid sizes $N$=128, 256, 512, 1024, and 2048. The error $e$ is computed as the discrete $L_1$ norm on the density residuals $\ell_1[\rho]$ using Equation 16, after shifting the computed density profile $\rho(x)$ in $x$ by $+\Delta x/2$. The data are shifted because at $t$=0, the $x$-velocity on the node located at $x$=0.5 is -1, while on the node at $x$=0.5–$\Delta x$, it is +1. Therefore, the initial location of the discontinuity is $x$=0.5–$\Delta x$/2. Convergence rates are computed using Equation 17.

Convergence studies for the magnetized Noh problem are performed for each of four configurations: (1) pure Lagrange-remap (LR) formulation without any DeBar correction, (2) LR formulation with only the kinetic-energy DeBar correction, (3) LR formulation with the full (kinetic + magnetic) DeBar correction, and (4) pure Lagrangian formulation. In configuration (3), total energy is conserved during remap. In configuration (1), only internal energy is conserved, as neither kinetic nor magnetic energy is advected conservatively. In configuration (2), total energy is again not conserved, as magnetic energy is not advected conservatively. It should be noted that the integrated total energy in the simulation is not constant in LR mode, but grows at a constant rate, because of the velocity boundary condition at $x$=0, 1.

The effect of these various energy conservation requirements on shock propagation in the magnetized Noh problem is shown in Figure 3(*a*). Profiles of the density at $t$=0.75 for each configuration, for grid size $N$=512, are shown along with the exact solution. In both of the configurations where total energy is not conserved in remap, erroneous shock speeds and post-shock states arise in the solution. The error is largest in the pure Lagrange-remap case, where no DeBar correction is applied (only internal energy is conserved). The speed of the fast MHD wave is drastically underestimated, and the density of the fluid after interaction with both the fast and slow MHD waves (the fully stagnated fluid) is overestimated by more than 10%. With the kinetic-energy DeBar correction, the disparity with respect to the exact solution is diminished, but remains significant, due to the failure to advect magnetic energy conservatively.

The failure to capture MHD shocks accurately when energy conservation is not maintained is illustrated even more clearly in the convergence data shown in Figure 3(*b*), which shows the trends of the density error $e=\ell_1[\rho]$ with respect to the grid size $N$. A straight dashed line indicates first-order convergence, which is the expected outcome, since the only degenerate mode in the problem is the stationary contact discontinuity at $x$=0.5. The corresponding convergence-rate data, computed using Equation 16, are shown in Table 1. Here we see that although the errors show very little difference between the configurations for coarse meshes, the disparity becomes dramatic at high resolution. Errors are more than an order of magnitude larger at $N$=2048 for the non-conserving cases than for the conserving cases. Further, the expected first-order convergence trend is achieved only in the conserving cases. This is confirmed also by the data in Table 1, which indicate that the convergence rates in the LR cases match the pure Lagrangian

rates to within a few percent only when both kinetic and magnetic energy are conservatively advected in remap by applying the full DeBar correction (the "total energy conserved" case).

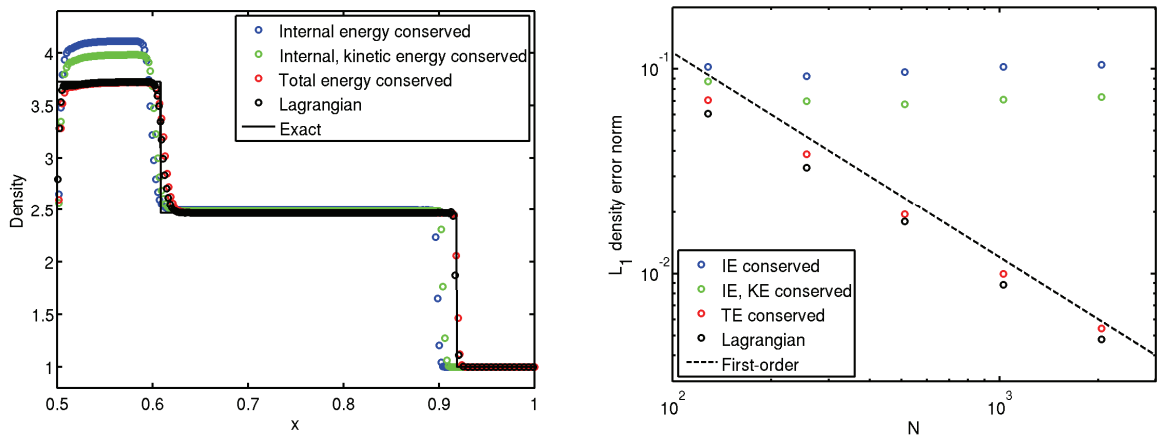


**Figure 3: Code verification results for the magnetized Noh problem at t=0.75. (a) Density profiles computed at *N*=512 for various remap configurations, compared to the exact solution, showing large errors in shock locations and post-shock states for cases where total energy is not conserved. (*b*) Convergence study results, showing first-order convergence of the density error $e=\ell_1[\rho]$ only in cases where total energy is conserved.**

Several other observations related to code verification may be made on the data shown in Figure 3. First, a dramatic, narrow expansion is clearly visible at the initial contact discontuity in all four scenarios, including the Lagrangian case. This "wall heating" is a persistent artifact of shock capturing using artificial viscosity, as has been thoroughly documented by Noh (1987). It can be diminished in magnitude only by using an odd number of elements in the *x*-direction, but cannot be eliminated without discarding artificial viscosity. It should also be noted that remap introduces significant dissipation at the shock fronts, so that in the full-DeBar-corrected case (total energy conserved), shocks have a slightly gentler slope than in the Lagrangian case (the shock spans more elements), and this results in the slightly larger error magnitudes plotted in Figure 3(*b*). This is observed for this problem regardless of whether the standard Van Leer advection algorithm is used, or the third-order method. In simulations at low resolution, this dissipation could tend to hide underlying errors due to energy conservation issues. An MHD-consistent artificial viscosity formulation would help to address this issue. Finally, we also note that, from a code verification standpoint, computing errors with respect to an independent exact solution was paramount, as trends in the error computed with respect to a highly-resolved

**Table 1. Density error convergence rates computed using Equation 17 for the magnetized Noh problem in various remap configurations.**

| Grid sizes | 128/256 | 256/512 | 512/1024 | 1024/2048 |
|---|---|---|---|---|
| IE conserved | 0.152 | -0.067 | -0.081 | -0.037 |
| IE, KE conserved | 0.319 | 0.046 | -0.069 | -0.046 |
| TE conserved | 0.880 | 0.979 | 0.965 | 0.880 |
| Lagrangian | 0.876 | 0.883 | 1.021 | 0.886 |

ALEGRA simulation indicated first-order convergence regardless of the remap configuration or grid size. (This may be regarded as convergence to a spurious, non-physical solution.)

**The magnetized Woodward-Colella problem**

In the second of the two verification problems, the magnetized Woodward-Colella problem, two sets of very strong MHD blast waves propagate into the medium from opposite ends of the domain. The medium is an ideal gas with $\gamma$=1.4 and $c_V$=1. These correspond to a set of fast and slow MHD modes in each direction for each discontinuity.

The problem is initialized on [0, 1] with three uniform states separated by discontinuities at $x$=0.1 and $x$=0.9:

$$\rho = 1.0$$

$$p = \begin{cases} 1000 & x < 0.1 \\ 0.01 & 0.1 < x < 0.9 \\ 100 & x > 0.9 \end{cases}$$

$$T = p/\rho/(\gamma - 1) = \begin{cases} 2500 & x < 0.1 \\ 0.025 & 0.1 < x < 0.9 \\ 250 & x > 0.9 \end{cases}$$

$$\mathbf{V} = 0$$

$$\mathbf{B} = 15(\hat{x} + \hat{y}),$$

where $T$ is the temperature. The problem is run to $t$=0.025 on meshes whose $x$-dimension is an integer multiple of 10, in order to preserve the correct initial discontinuity positions. This is identical to the problem simulated by Woodward and Colella (1984), except that a uniform, oblique field B=15 $(\hat{x} + \hat{y})$ is imposed, and the solution is analyzed at $t$=0.025 instead of $t$=0.038. Shock interactions here, however, are not as strong, because the shock energy is carried by four waves that are generated from the initial two discontinuities, rather than by only two, and because at $t$=0.025, only the fast MHD waves have interacted.

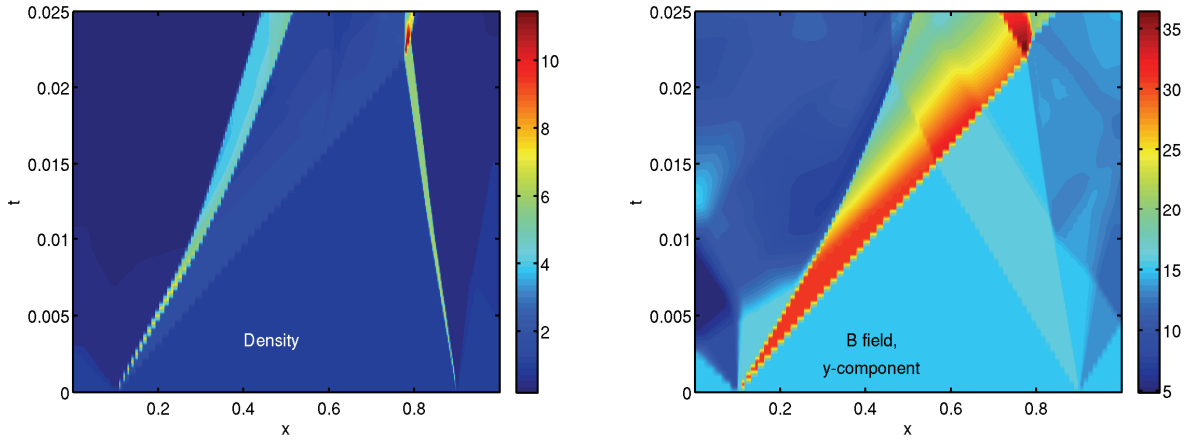


**Figure 4: ALEGRA results at N=4096 for the magnetized Woodward-Colella problem, plotted in ($x$,$t$) space. MHD waves propagate in both directions from initial discontinuities in pressure and temperature at $x$=0.1 and 0.9. Left: density; right: $y$-component of B field.**

The propagation and interaction of these waves is shown in Figure 5, where ALEGRA results for this problem at $N$=4096 are plotted in ($x$,$t$) space. Unlike the magnetized Noh problem, which is essentially a stagnation flow, the magnetized Woodward-Colella problem is pressure-driven,

starting from a quiescent state. MHD waves propagate into the stagnant, magnetized medium, transforming internal energy into kinetic and magnetic energy. This provides a similar test of energy conservation capability as the magnetized Noh problem, but adds the much greater complexity of MHD wave interactions, due to both the convergent shocks and the rarefaction waves reflected at the boundaries.

**Magnetized Woodward-Colella problem setup.** As in the magnetized Noh problem, the magnetized Woodward-Colella problem is set up on a uniform three-dimensional mesh of dimensions $N\times2\times2$, with hexahedral elements of aspect ratio 1. The blast waves propagate in the $\pm x$-directions, and periodic boundary conditions are imposed in the $y$- and $z$- directions. Reflecting boundary conditions are imposed at the ends of the domain (constant-$x$ bounding surfaces), consistent with the purely hydrodynamic Woodward-Colella problem. In this case, the total energy in the system should remain constant over time. For the present magnetized problem, reflecting boundaries are implemented at $x$=0, 1 by requiring that the products ($v_x v_y$) and ($B_x B_y$) have the same symmetry about a boundary. Then, since $B_x$ has even symmetry by definition, and $v_x$ must have odd symmetry to support wave reflection, all of the components of **B** must have odd symmetry about the boundary, and all of the components of **V** must have even symmetry. For this problem, these requirements can be maintained by imposing zero-displacement boundary conditions on all three velocity components at $x$=0,1, and imposing symmetric (projection) boundary conditions for the components of **B**. (In ALEGRA, the latter is maintained implicitly in the finite-element formulation.) Again, we note that the specification of correct boundary conditions for the transverse components of the velocity is paramount for the success of the simulation, since subtle errors in $B_y$ and $v_y$ may arise otherwise, which lead to the loss or gain of energy in the simulation over time.

Tensor artificial viscosity, with both linear and quadratic components, is included for shock capturing, with a linear coefficient of 0.5 and a quadratic coefficient of 2.0. The note in Section 5.1 regarding MHD inconsistency of the artificial viscosity scheme applies here as well. These simulations are also performed using the third-order advection scheme in the remap algorithm (rather than the default second-order van Leer algorithm), for reasons that are discussed below.

A reference solution for this problem is computed using the ideal-MHD Eulerian Godunov code *Athena* (see Gardiner and Stone, 2005 and Stone and Gardiner, 2007). No exact solution is available for this problem, and very accurate solutions may be computed at relatively little expense using a direct Eulerian scheme for a problem such as this, where the perfect-gas equation of state is used. Gardiner and Stone (2005) demonstrate second-order convergence in solutions computed using *Athena* for linear MHD wave propagation, and provide code verification results additionally for a number of other ideal-MHD test problems. Solutions computed for the magnetized Woodward-Colella problem at $t$=0.025 and grid size $N$ using *Athena* exhibit near-first-order convergence of the density error norm with respect to the solution at grid size $2N$, up to $N$=10,000. For a range of meshes between $N$=1250 and $N$=10, 000, a mean convergence rate $p$=0.84±0.04 is observed, and the error at $N_f$=10,000 is $e_f$=0.0023. Preliminary analysis of ALEGRA solutions indicates smallest numerical errors of approximately $7\times10^{-3}$. Richardson extrapolation suggests, then, that error in the *Athena* solution will be at least one order of magnitude smaller than the smallest errors in the ALEGRA simulations for a mesh size

$N_R = N_f\,(e_f/7\times10^{-4})^{1/p} \approx 42{,}000.$

Therefore, we generate a reference solution using *Athena* on an even larger mesh: $N$=52,000; errors in ALEGRA solutions for the magnetized Woodward-Colella problem are computed with respect to this solution.

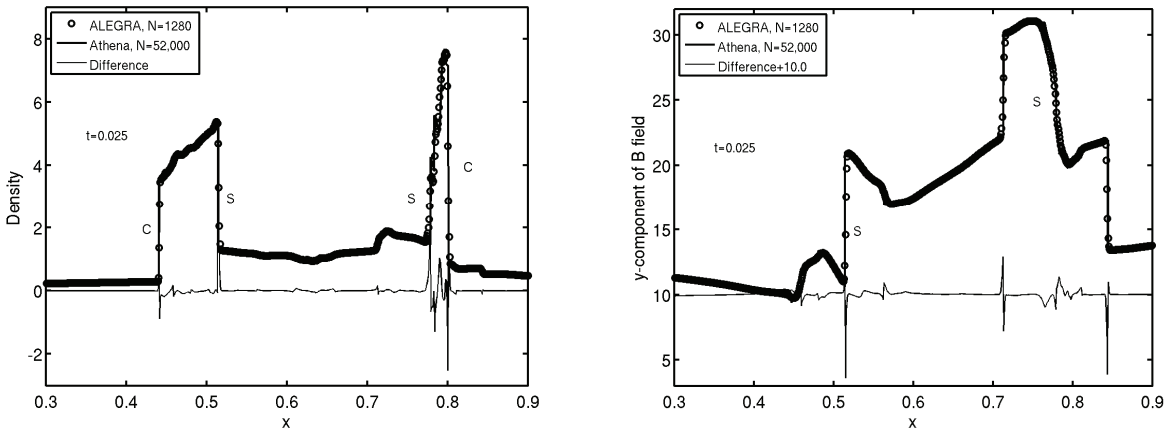


**Figure 5: Sample ALEGRA results at N=1280 and t=0.025 for a subregion of the domain in the magnetized Woodward-Colella problem, plotted with the reference *Athena* solution. Left: density; right: *y*-component of B field. Contact discontinuities are indicated by "C" and slow-mode MHD waves by "S." The difference betwen the two solutions is plotted as a lighter trace.**

Profiles of density and the *y*-component of the **B** field are shown for a subregion of the domain in Figure 6, including the ALEGRA solution for $N$=1280, and the *Athena* solution for $N$=52,000. A complex series of nonlinear MHD waves is seen in the solution profiles, dominated by two structures, particularly evident in the density profile, that are moving toward each other. The outermost edge of each of the structures in the density profile are the original contact discontinuities (marked "C"), and the inner edges of the structures are the remnants of the slow-mode MHD waves (marked "S").

**Energy conservation in the magnetized Woodward-Colella problem.** As in the case of the magnetized Noh problem, a convergence study sequence is performed for this problem using each of the four remap configurations. In each convergence study, the magnetized Woodward-Colella simulation is run to $t$=0.025 for grid sizes $N$=160, 320, 640, 1280, 2560, and 5120. We note that each grid size must be an integer multiple of 10 in order to ensure that the initial discontinuities – in the element-centered variables pressure and density – are each located precisely on an element boundary, at $x$=0.1 and 0.9. The density error $e$ is computed for each of these cases, again, as $e=\ell_1[\rho]$ with using Equation 16, and convergence rates are computed using Equation 17.

The four remap configurations outlined above are simulated here as well: (1) LR with no DeBar correction, (2) LR with DeBar correction for kinetic energy only, (3) LR with full DeBar correction, and (4) pure Lagrangian formulation. The effect of these remap configurations on the solution in the magnetized Woodward-Colella problem is shown in Figure 7(*a*), where, for simplicity, only the density profiles on [0.43, 0.53] are plotted. Similarly to the results shown in Figure 3(*a*), the remap configurations that do not advect all three forms of the energy conservatively fail to reproduce the correct nonlinear wave speeds and shock jump conditions seen in the reference density profile. The uncorrected Lagrange-remap case shows the most dramatic error, and although applying the kinetic-energy DeBar correction reduces the error, an acceptable level of agreement with the highly resolved Eulerian Godunov solution and with the pure Lagrangian result is only achieved when the full DeBar correction is applied.

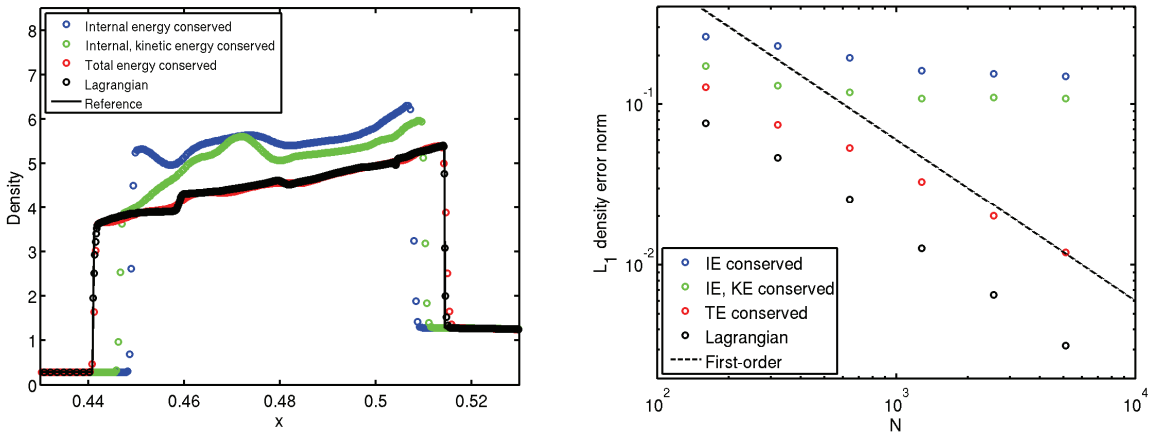


**Figure 6: Code verification results for the magnetized Woodward-Colella problem at t=0.025. (a) Density profiles computed at $N$=1280 for various remap configurations, compared to the reference solution, showing large errors in shock locations and post-shock states for cases where total energy is not conserved. (*b*) Convergence study results, showing convergence of the density error $e=\ell_1[\rho]$ at a rate of $p$=0.75 only in cases where total energy is conserved.**

The convergence behavior of the solutions in these cases is shown in Figure 7(*b*), which plots trends in the density error $e=\ell_1[\rho]$ with respect to the grid size $N$, with a straight dashed line denoting behavior proportional to $N^{-0.75}$. Based on the analysis of Banks *et al.* (2008), a convergence rate of $p=r/(r+1)=0.75$ is the expected outcome here because of the presence of contact discontinuities that move across the mesh, and the use of the third-order remap algorithm ($r$=3). (Note that first-order convergence is still expected in the Lagrangian simulation, since contacts are represented exactly in that case.) The corresponding convergence rates are shown in Table 2. The results again show diverging trends based on whether the total energy is conserved, and error magnitudes that grow as the energy conservation requirements are successively relaxed. Very poor convergence in the non-conserving cases reflects gross shock propagation errors evident in Figure 7(*a*), and we see that with total energy conservation enforced by use of the full (kinetic + magnetic) DeBar correction, distinctly improved convergence behavior is observed. Only when the full DeBar correction is implemented do convergence rates in the LR simulations approach the expected value.

**Table 1. Density error convergence rates computed using Equation 17 for the magnetized Woodward-Colella problem in various remap configurations.**

| Grid sizes | 160/320 | 320/640 | 640/1280 | 1280/2560 | 2560/5120 |
|---|---|---|---|---|---|
| IE conserved | 0.194 | 0.245 | 0.258 | 0.071 | 0.047 |
| IE, KE conserved | 0.403 | 0.129 | 0.135 | -0.023 | 0.024 |
| TE conserved | 0.773 | 0.480 | 0.700 | 0.709 | 0.750 |
| Lagrangian | 0.717 | 0.855 | 1.022 | 0.954 | 1.031 |

Based on the data in Figure 7, we observe again that LR solutions generally exhibit a greater degree of dissipation than the pure-Lagrangian simulations. This accounts in part for the larger error magnitudes and lower convergence rates seen in the LR results in Figure 7 compared to the Lagrangian results, even with third-order advection and the full DeBar correction activated. This

disparity is noticeably greater in the magnetized Woodward-Colella problem than in the magnetized Noh problem, due to the much stronger variations in pressure, density, and transverse B-field associated with interacting shocks. We speculate that the origin of this spurious dissipation lies with the artificial viscosity algorithm, which, as previously mentioned, is not MHD-consistent. Also, a wall-heating effect is similarly present in these simulations (appearing on the right-most slow-mode wave), as in the magnetized Noh simulations, though its effect here is much less significant.

**Conclusions**

By incorporating a correction for the magnetic energy similar to that originally proposed by DeBar (1974), finite-element MHD simulations in ALEGRA are able to maintain conservation of total energy while operating with a Lagrange-remap framework. Code verification results based on two classical shock-hydrodynamics test problems adapted for use as MHD-shock test problems indicate that near-first-order convergence to exact or highly accurate reference solutions is achieved when total-energy conservation is maintained, either by use of a purely Lagrangian scheme, or by use of the full DeBar correction in Lagrange-remap calculations. Further, the results indicate that acceptable convergence behavior is obtained for these problems *only* when total-energy conservation is maintained. Though the DeBar correction has been widely used to maintain total-energy conservation in pure hydrodynamic or solid-dynamic Lagrange-remap numerical methods, this study suggests that the magnetic extension should be incorporated into MHD Lagrange-remap methods as well.

These observations are founded on insights provided by order verification, which has proven to be a powerful tool for exposing underlying inconsistencies in the methods studied here. Non-convergence of solutions provides a key indicator for code verification, particularly when error magnitudes alone are insufficient as a criterion for differentiating between acceptable and unacceptable results. Further, convergence criteria based on errors with respect to an independent exact or highly accurate solution provide insights that are hidden when errors with respect to a refined mesh are computed. Care must be taken in computing these norms; volume-weighting of error norms is essential in many cases, and the centering of variables poses certain requirements on the meshes that may be used and the frame of reference within which independent solutions may be compared. With all of these requirements address, the complete verification study yields tangible evidence of the consistency and accuracy of the numerical methods used here in ALEGRA, and it is anticipated that future *validation* tests will yield further insight into the usefulness of these methods in MHD applications.

**References**

Banks, J. W., Aslam, T., and Rider, W. J. "On sublinear convergence for linearly degenerate waves in capturing schemes." *J. Comp. Phys.*, 227:6985–7002 (2008).

Benson, D. J. "Computational methods in Lagrangian and Eulerian hydrocodes." *Computer Methods in Applied Mechanics and Engineering*, 99:235–394 (1992).

Benson, D. J. "Momentum advection on a staggered mesh." *J.Comp. Phys.*, 100:143–162 (1992).

DeBar, R. "Fundamentals of the KRAKEN code." Technical report, LLNL, UCIR-760 (1974).

Dolbow, J., Mosso, S.J., *et al*. "Coupling volume-of-fluid based interface reconstructions with the extended finite element method." *Comput. Methods Appl. Mech. Engrg.*, 197:439-447 (2008).

Evans, C. R. and Hawley, J. F. "Simulation of magnetohydrodynamic flows: a constrained transport method." *Ap. J.*, 332:659–677 (1988).

Gardiner, T. A. and Stone, J. M. "An unsplit Godunov method for ideal MHD via constrained transport." *J. Comp. Phys.*, 205:509–539 (2005).

Lax, P.D. *Hyperbolic Systems of Conservation Laws and Mathematical Theory of Shock Waves*. (SIAM, Philadelphia, PA, 1973).

Van Leer, B. "Towards the ultimate conservative difference scheme V. A second-order sequel to Godunov's methods." *J. Comp. Phys.*, 32:101–136 (1979).

McGlaun, J. M., Thompson, S. L., and Elrick, M. G. "CTH: a three-dimensional shock wave physics code." *Int. J. Impact Engng.*, 10:351–360 (1990).

Mosso, S. J., Garasi, C. J., and Drake, R. R. "A smoothed two- and three-dimensional interface reconstruction method" *Comput. Visual. Sci.*, online:DOI 10.1007/s00791-008-0108-y (2008).

Noh W. F. "Errors for calculations of strong shocks using an artificial viscosity and an artificial heat flux." *J. Comp. Phys.*, 72:78–120 (1987).

Ober, C. C. and Shadid J. N. "Studies on the accuracy of time-integration methods for the radiation-diffusion equations." *J. Comp. Phys.*, 195:743–772 (2004).

Peery, J. S. and Carroll, D. E.. "Multi-material ALE methods in unstructured grids." *Comput. Methods Appl. Mech. Engrg.*, 187:591–619 (2000).

Pember, R. and Anderson, R. "A comparison of staggered-mesh Lagrange plus remap and cell-centered direct Eulerian Godunov schemes for Eulerian shock hydrodynamics." Technical report, LLNL, UCRL-JC-139820 (2000).

Robinson, A. C. and Garasi, C. J.. "Three-dimensional z-pinch wire array modeling with ALEGRA-HEDP." *Comput. Phys. Commun.*, 164:408–413 (2004).

Robinson, A. C., Rider, W. J., *et al.* "ALEGRA: An arbitrary Lagrangian-Eulerian multimaterial, multiphysics code." In *Proceedings of the 46th AIAA Aerospace Sciences Meeting, Reno, NV*, AIAA-2008-1235 (2008).

Roe, P. L. and Balsara, D. S. "Notes on the eigensystem of magnetohydrodynamics." *SIAM J. Appl. Math.*, 56(1):57–67 (1996).

Ryu, D. and Jones, T. W. "Numerical magnetohydrodynamics in astrophysics: algorithm and tests for one-dimensional flow." *Ap. J.*, 442:228–258 (1995).

Stone, J. M. and Gardiner, T. A. "Nonlinear evolution of the magnetohydrodynamic Rayleigh-Taylor instability." *Phys. Fluids*, 19(094104) (2007).

Tadmore, E. "Approximate solutions of nonlinear conservation laws: Convergence rate estimates" (Chapter 1.4). In A. Quarteroni, editor, *Advanced Numerical Approximation of Nonlinear Hyperbolic Equations*, pages 109–137, (Springer-Verlag, Berlin, 1998).

Woodward, P. and Colella, P.. "The numerical simulation of two-dimensional fluid flow with strong shocks." *J. Comp. Phys.*, 54:115–173 (1984).

Youngs, D. L. "The Lagrangian remap method" (Chapter 4c). In F. F. Grinstein, L. G. Margolin, and W. J. Rider, editors, *Implicit Large Eddy Simulation*, pages 147–153 (Cambridge Univ. Press, 2007).

**Acknowledgements**

*Sandia is a multiprogram laboratory operated by Sandia Corporation, a Lockheed Martin Company, for the United States Department of Energy's National Nuclear Security Administration under Contract DE-AC04-94-AL85000.*